available at www.sciencedirect.com

ScienceDirect

journal homepage: www.elsevier.com/locate/ijrefrig

Numerical simulation of the transient heat transfer during nucleate boiling of refrigerant HFE-7100

Christian Kunkelmann [a], *Peter Stephan* [a,b,*]

[a] *Institute for Technical Thermodynamics, Technische Universität Darmstadt, Petersenstraße 30, D-64287 Darmstadt, Germany*
[b] *Center of Smart Interfaces, Technische Universität Darmstadt, Petersenstraße 32, D-64287 Darmstadt, Germany*

Dedicated to Professor Dr.-Ing. Dr.h.c.mult. Karl Stephan on the occasion of his 80th birthday.

ARTICLE INFO

Article history:
Received 22 March 2010
Received in revised form
8 July 2010
Accepted 10 July 2010
Available online 16 July 2010

Keywords:
Boiling model
Transient heat transfer
Contact line evaporation
Refrigerant HFE-7100

ABSTRACT

The transient heat transfer during nucleate boiling of refrigerant HFE-7100 is investigated numerically and the results are compared to experimental data. The Volume-of-Fluid solver of the OpenFOAM CFD package was modified and extended for the numerical simulation of single bubble boiling. The model tracks the bubble shape during growth, departure and vertical rise and incorporates evaporation at the liquid–vapor interface as well as microscale heat transfer at the 3-phase contact line. The simulation results give insight into the transient heat transfer between the solid wall, the superheated liquid layer and the growing vapor bubble. The boundary conditions have been chosen according to temporally and spatially highly resolved experimental investigations. Global parameters such as bubble size and mean wall superheat as well as local phenomena such as the cooling of the heater at the contact line are in good agreement to the experimental data.

Simulation numérique du transfert de chaleur transitoire lors de l'ébullition nucléée du frigorigène HFE-7100

Mots clés : Ébullition nucléée ; Régime transitoire ; Transfert de chaleur ; HFE-7100 ; Modélisation-simulation

1. Introduction

Boiling is one of the most efficient ways to achieve high heat fluxes at a reasonable wall superheat. The high heat transfer coefficients that can be achieved are of utmost interest for many applications in the field of refrigeration, cooling of electronic devices as well as power generation. In a large number of applications, in particular cooling for high performance electronics, the devices become smaller while the heat dissipation and the maximum admissible temperature remain the same. Hence, the required heat transfer coefficients can easily exceed the ones that can be achieved with single-phase heat transfer. Boiling can be an alternative, but there is need for accurate prediction of heat transfer coefficient and critical heat flux. Unfortunately, many of the physical phenomena that occur in boiling and their interaction are still not well understood. Consequently, non-empirical predictive tools are rare.

* *Corresponding author*. Tel.: +49 6151 163159; fax: +49 6151 166561.
E-mail address: pstephan@ttd.tu-darmstadt.de (P. Stephan).
0140-7007/$ – see front matter © 2010 Elsevier Ltd and IIR. All rights reserved.
doi:10.1016/j.ijrefrig.2010.07.013

Nomenclature

c	Specific heat capacity, J kg^{-1} K^{-1}
F	Volume fraction
$\vec{f}$	Momentum source term, N m^{-3}
h_{lv}	Enthalpy of vaporization, J kg^{-1}
$\dot{h}$	Energy source term, W m^{-3}
p	Pressure, Pa
q	Heat flux, W m^{-2}
Q	Heat flow, W
$\vec{S}_{int,i}$	Area vector of liquid–vapor interface in cell i, m^2
t	Time, s
T	Temperature, K
$\vec{u}$	Velocity, m s^{-1}
V	Volume, m^3
$\vec{w}$	Artificial speed for reinitialization of level-set field, m s^{-1}

Greek symbols

δ	Thickness of heating foil, m
ε	Typical grid size, m
λ	Heat conductivity, W m^{-1} K^{-1}
μ	Dynamic viscosity, Pa s
Φ	Level set (distance to interface), m
ρ	Density, kg m^{-3}
$\dot{\rho}$	Mass source term, kg m^{-3} s^{-1}
τ	Artificial time for reinitialization of level-set field, s

Subscripts

cl	Contact line
el	Electric
g	Gravity
int	Interface
l	Liquid
lat,att	Latent heat, attached bubble
lat,det	Latent heat, detached bubble
sat	Saturation
ST	Surface tension
v	vapor

The difficulties in both the experimental and numerical investigation of boiling phenomena are due to the small length scales which have a non-negligible impact on the bubble growth (e.g. the microscale evaporation at the contact line), the highly dynamic nature of boiling heat transfer and the complexity of the transient heat transfer between solid, liquid and vapor. An accurate prediction tool for nucleate boiling in the isolated bubble regime has been developed by Fuchs et al. (2006). The model uses a Langrangian mesh that follows the motion of the liquid–vapor interface and captures the microscale heat transfer according to the work of Stephan and Busse (1992). The major drawbacks of the Lagrangian approach are the assumption that the bubble is spherical until it detaches from the heating wall and the incapability of the model to simulate interaction between multiple bubbles. During the last years, very robust methods like Volume-of-Fluid (VOF) and Level-Set (LS) which can capture a moving interface on a fixed grid have been developed. Unfortunately, the modeling of phase change is more complex in such an approach because the position of the liquid–vapor interface does not coincide with a boundary of the computational domain. In a number of numerical works LS has been used to simulate boiling of water in different flow conditions (Son et al., 1999; Wu et al., 2007; Li and Dhir, 2007). The authors found good agreement to experimental data. However, only boiling of water on isothermal heating walls was investigated. Kunkelmann and Stephan (2009) implemented a boiling model into the CFD package OpenFOAM (Weller et al., 1998) and performed preliminary simulations for boiling of HFE-7100. The model takes into account the transient heat conduction in the solid wall. Good qualitative agreement to high-resolution measurements was found.

Nucleate boiling of refrigerants has been investigated in a number of experiments. Demiray and Kim (2004) and Myers et al. (2005) used a microheater array to boil FC-72 and investigated the local temperature and heat flux at the wall beneath the growing bubbles. The authors observed a high local heat flux in the contact line region or, depending on the boundary condition which is imposed via a microheater array, a strong cooling effect. Another experimental work providing deep insights into the boiling process has been performed by Wagner et al. (2007) with HFE-7100. A thin steel heating foil with an artificial nucleation site was used to generate single bubbles. The temperature of the heating foil was measured with a high-speed infrared camera. High heat fluxes and strong cooling at the contact line region could clearly be seen.

The aim of the present work is to numerically investigate boiling of HFE-7100 at 500 mbar on a steel heating foil according to the experiment of Wagner et al. (2007). The boiling model which has recently been implemented in OpenFOAM (Kunkelmann and Stephan, 2009) is extended and modified in order to allow the simulation of boiling in real conditions. The results of the simulation are qualitatively and quantitatively compared to the experimental data.

2. Numerical method

In this section, the numerical basics of the boiling model are briefly described. More detailed information on the numerical method can be found in a previous publication (Kunkelmann and Stephan, 2009).

2.1. Governing equations

The equations that need to be solved in the boiling model are the conservation equations for mass, momentum, energy and volume fraction:

$$\nabla\cdot(\rho\vec{u}) = \dot{\rho}, \tag{1}$$

$$\frac{\partial\rho\vec{u}}{\partial t} + \nabla(\vec{u}\cdot\rho\vec{u}) = -\nabla p + \nabla\cdot(\mu\cdot\nabla\vec{u}) + \vec{f}_{ST} + \vec{f}_{g}, \tag{2}$$

$$\frac{\partial\rho cT}{\partial t} + \nabla\cdot(\vec{u}\cdot\rho cT) = \nabla\cdot(\lambda\cdot\nabla T) + \dot{h}, \tag{3}$$

$$\frac{\partial F}{\partial t} + \nabla \cdot (\vec{u} \cdot F) = \frac{\dot{\rho}}{\rho} F. \tag{4}$$

The volume fraction field determines the liquid volume fraction in each cell. It has a value of 0 in all vapor cells, a value of 1 in all liquid cells and a value between 0 and 1 in cells that are cut by the liquid–vapor interface. The volumetric forces $\vec{f}_{ST}$ and $\vec{f}_{g}$ on the right-hand side of Eq. (2) account for surface tension and gravity, respectively, while the source terms on the right hand sides of Eqs. (1), (3) and (4) account for the phase change. The calculation of the source term field is explained below. Mass is removed on the liquid side of the interface and reappears on the vapor side. In spite of the local mass source terms, the mass is globally conserved.

2.2. Phase change model

In a previous work (Kunkelmann and Stephan, 2009) the phase change has been modeled according to the original approach of Hardt and Wondra (2008). The simulation of a validation case has shown that a very fine grid (cell size below 1 μm) is required in order to capture the evaporation correctly. A number of modifications were performed in order to permit the simulation of nucleate boiling on more coarse grids (cell size of a few microns) with the same level of accuracy. The most important change is the coupling of the VOF method to an LS approach. While the VOF field does not contain information about the exact position of the interface, the LS field represents the geometric distance to the interface and permits a more precise interface reconstruction. The LS field is estimated from the VOF field in each time step and corrected according to the approach of Sussman et al. (1999) to be a signed distance function:

$$\Phi = (2 \cdot F - 1) \cdot \varepsilon, \tag{5}$$

$$\frac{\partial \Phi}{\partial \tau} + \vec{w} \cdot \nabla \Phi = \mathrm{sign}(\Phi), \tag{6}$$

$$\vec{w} = sign(\Phi) \cdot \frac{\nabla \Phi}{|\nabla \Phi|}. \tag{7}$$

The exact reconstruction of the interface is crucial for the calculation of the local evaporation source term which depends on the local temperature gradient and the area of the interface in each cell:

$$\dot{\rho}_{0,i} = \frac{\lambda_l \cdot \nabla T \cdot \vec{S}_{int,i}}{h_{lv} V_i} = \frac{\lambda_l \cdot (T_i - T_{sat}) \cdot S_{int,i}}{h_{lv} \Phi_i V_i}. \tag{8}$$

Once the local source terms are determined in all cells, the resulting field is smeared and the smooth source-term distribution $\dot{\rho}$ is obtained according to the approach of Hardt and Wondra (2008).

2.3. Contact line evaporation

The microscale heat transfer at the contact line is governed by physics that act on a length scale which cannot be resolved by the numerical mesh. Therefore, the contact line heat transfer has to be treated by a sub-model that interacts with the simulation. In a microscopic scale there is no actual contact line, as can be seen in Fig. 1a. The adsorbed film region where liquid molecules are attracted by adhesion forces and stick to the wall without evaporating and the macro region where adhesion forces are negligible are connected by the micro region. Stephan and Busse (1992) derive a fourth-order differential equation for this region which can be solved numerically. The results (film thickness, curvature, heat flux and integrated heat flux) are shown exemplarily in Fig. 1b. For a given fluid they depend mainly on the wall superheat and can be correlated prior to the simulation. The most important parameters for coupling the sub-model to the simulation are the integrated heat flux (heat flow per unit contact line length) and the local wall superheat at the contact line. The local wall superheat is taken from the simulation and serves as input parameter for the sub-model. The sub-model calculates the integrated heat flux which is then multiplied by the contact line length and used as a boundary condition in the simulation. More details on the procedure can be taken from Kunkelmann and Stephan (2009).

3. Results and discussion

Wagner et al. (2007) investigated boiling of HFE-7100 at 500 mbar on a steel heating foil with a thickness of 50 μm. An

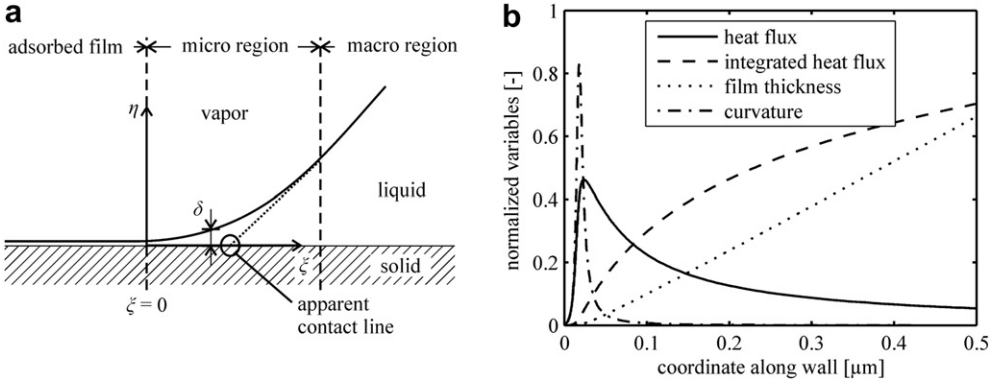

Fig. 1 – (a) Definition of the micro region and the apparent contact line (b) Development of normalized heat flux (normalized by 50 MW m^{-2}), integrated heat flux (normalized by 5 W m^{-1}), film thickness (normalized by 0.5 μm) and curvature (normalized by 50 μm^{-1}) in the micro region. Results obtained for HFE-7100 at 500 mbar and a wall superheat of 15 K.

artificial nucleation site on the heating foil enabled the generation of single bubbles at a prescribed position. The steel foil is heated by an electric current resulting in a heat flux of 5400 W m^{-2}. The authors state that the heat transfer to the surrounding air at the back side of the foil can be neglected compared to the heat transfer to the boiling fluid. The bubble shape is observed with a high-speed camera from the side, while the temperature of the steel heating foil was measured with a high-speed infrared camera from below. The authors observe periodic bubble events with a bubble growth time of 13 ms and a departure diameter of 1.9 mm. The mean superheat of the heating foil is around 15 K. The temporal and spatial resolutions of the experimental apparatus allow observing the local cooling and the high heat fluxes at the contact line. At the contact line the authors measure a temperature decrease of about 1.5 K and a local heat flux peak of about 150 kW m^{-2}. In the following, the setup of the simulation is explained and its results are shown and compared to experimental data.

3.1. *Setup and convergence of the simulation*

At the current state of development, the boiling model does not include sub-models for contact angle dynamics and the waiting time before the nucleation of a new bubble. Therefore, constant values of 40° for the contact angle and of 25 ms for the waiting time have been chosen based on experimental observations. The geometric setup of the simulation and the most relevant boundary conditions are shown in Fig. 2. The initial temperature profile in the liquid layer close to the heating wall is assumed to be linear with a thickness of 0.18 mm while the heating wall is assumed to have an initial constant superheat of 15 K. These choices are arbitrary, but the simulation of several consecutive bubble cycles permits to reach a periodic regime which is independent of the initial conditions. The convergence of the temperature profile in the liquid phase close to the heating wall is shown in Fig. 3. The

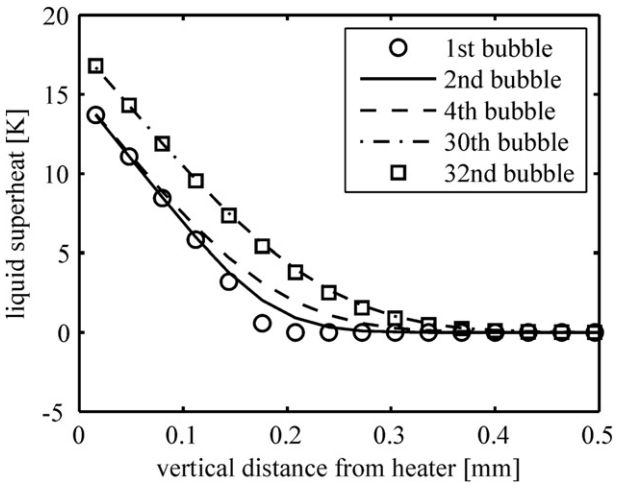

Fig. 3 – Temporal development of the temperature profile in the liquid at the outer boundary of the computational domain. The temperature profiles are taken at the moment of nucleation of different bubbles.

temperature profiles are taken at different nucleation events. The temperature profile changes significantly during the first bubble cycles. However, after several cycles the change becomes smaller and the temperature field in the superheated liquid layer becomes periodic (i.e. no change between 30th and 32nd bubble). The temporal evolution of the mean heater temperature is plotted in Fig. 4. The mean wall superheat is obtained by spatially averaging the instantaneous wall superheat in a circular area with a radius of 1 mm around the nucleation site. Again, we can state that a periodic regime is reached after several bubble cycles. In order to obtain valid results the simulation is continued until all parameters are periodic. In the case which is the subject of this paper periodicity is reached after about 40 bubble cycles.

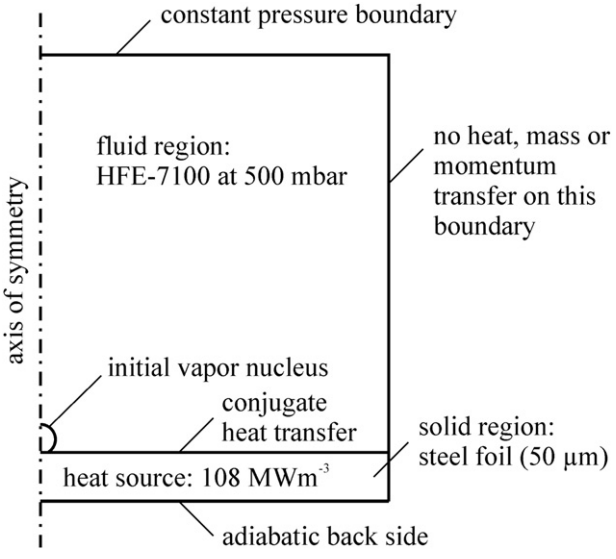

Fig. 2 – Sketch of the computational domain showing the most relevant boundary conditions.

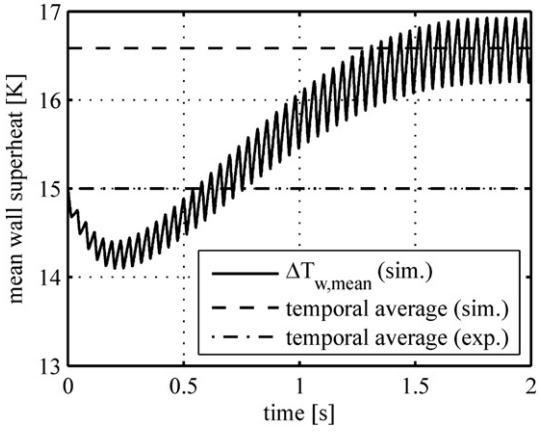

Fig. 4 – Temporal development of instantaneous, spatially averaged wall temperature (in a circular area with a radius of 1 mm around the nucleation site), temporal average of instantaneous development is obtained for the last five bubble cycles and compared to experimental data (Wagner et al., 2007).

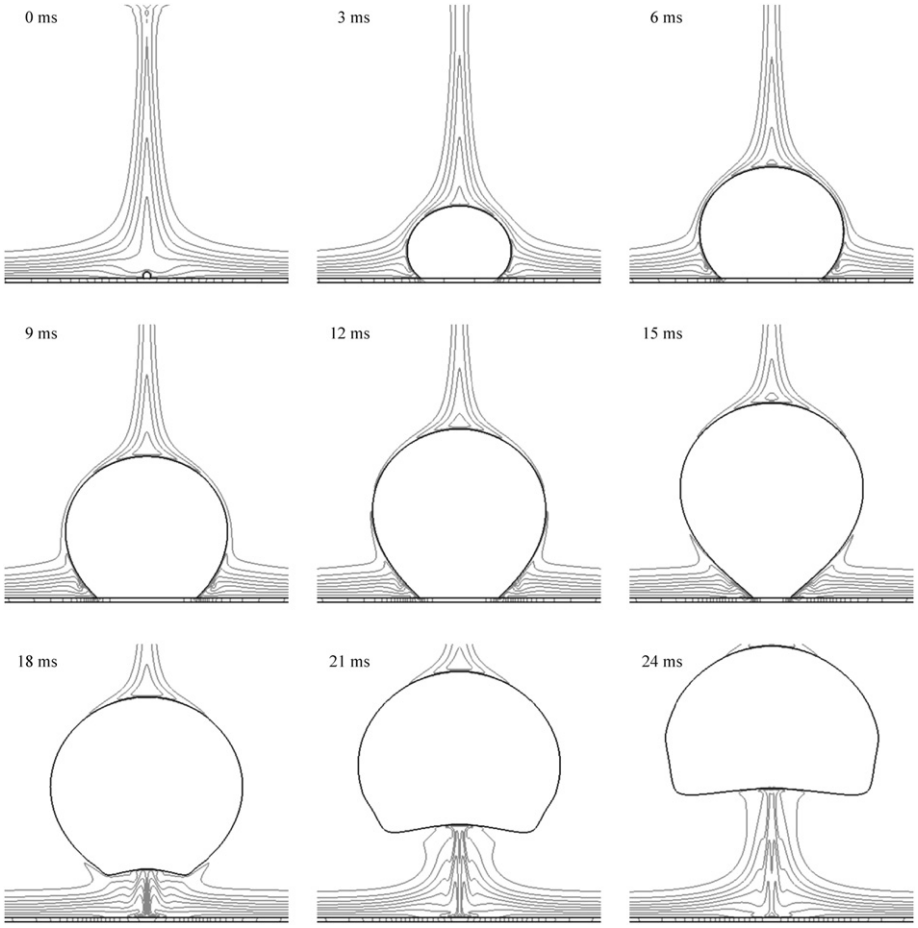

Fig. 5 – Bubble contour and isotherms during one bubble cycle (temperature step between isotherms: 2 K in liquid and 0.2 K in solid).

3.2. *Simulation results and comparison to experiment*

The bubble contour and temperature field during one bubble cycle in the periodic regime is shown in Fig. 5. In a first step, the departure diameter and growth time of the simulated bubbles in the periodic regime are compared to experimental data. The growth time converges to a value of 16 ms while the departure diameter converges to a value of 2.3 mm. Both results are around 20% above the values obtained experimentally. Due to the high complexity of the boiling process, this result is still very promising. Possible reasons for the deviation are given below. In a next step, the instantaneous, spatially averaged wall superheat is investigated and compared. Apart from its development with time, also the temporal average (last five bubble cycles) of the wall superheat is plotted in Fig. 4. The value is only 10% above the experimental value.

The total heat flow transferred between solid and fluid (Q_{heater}), the latent heat consumption of the bubble ($Q_{lat,att}$ and $Q_{lat,det}$ for attached and detached bubble, respectively), the contact line heat transfer (Q_{cl}) and the sum of contact line heat transfer and transient conduction ($Q_{cl} + Q_{tc}$) are plotted versus time in Fig. 6. The latent heat consumed by the bubble rises rapidly to a maximum value of around 0.4 W which is in excellent agreement to experimental observations. Then the value drops, but there is still evaporation even after bubble departure. This is due to the superheated liquid which is sucked away from the wall by the departing bubbles. The contact line heat transfer is approximately proportional to the contact line length and thus decreasing during detachment. However, transient conduction in the near contact line region keeps the local heat transfer high. The phenomenon of transient conduction will be further specified below. Temporally integrated over a full bubble, the near contact line heat transfer including transient heat conduction provides around 20% of the total heat consumed by the bubble. Wagner et al. (2007) state a value of 20–30%. Hence, the bubble gets around 70–80% of the heat from the superheated liquid layer. Therefore, the heat consumption of the bubble lies above the total heat provided by the heater during a significant duration of the bubble cycle. The liquid superheat is recharged during the waiting time.

Wagner et al. (2007) measured the temperature on the adiabatic back side of the heating foil and used an energy balance to obtain the local heat flux that is transferred from solid to fluid:

$$q_{\mathrm{Fluid}} = q_{\mathrm{el}} - \delta \cdot \left[\frac{\partial \rho c T}{\partial t} - \nabla \cdot (\lambda \cdot \nabla T) \right]. \tag{9}$$

The simulation results are post-processed in the same way in order to obtain comparable results for the local wall heat flux. The heat flux can also be obtained directly at the

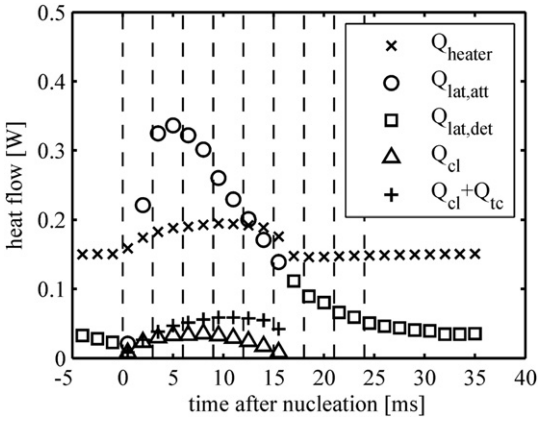

Fig. 6 – Heat flows during one bubble cycle (vertical dashed lines indicate the instances shown in Fig. 5).

solid–fluid interface in the simulation, but these results do not incorporate the damping of the signal in the heating foil and cannot be compared to the experimental observations. The result of Eq. (9) at three different times during one bubble cycle is shown in Fig. 7. A clear peak is visible at the position of the contact line. The slight asymmetric shape is due to the motion of the contact line and does not occur when the contact line is stagnating at the position of the maximum foot diameter (dashed line). Wagner et al. (2007) measured a peak heat flux of around 150 kW m^{-2} when the bubble foot diameter is growing. This result matches very well with the simulation result for the growing foot diameter. However, in the experimental data, the peak becomes very small when the bubble foot radius reaches its maximum value and during detachment (not shown in Fig. 7). The simulation results show a different behavior: The maximum peak value grows slightly during the entire bubble growth and detachment process. A possible explanation for this deviation is given below. The corresponding temperature profiles on the front and back side

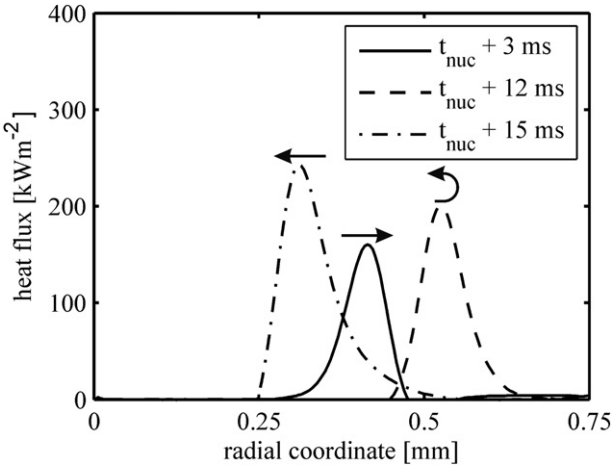

Fig. 7 – Local wall heat flux in different situations during bubble growth obtained from simulation (receding, stagnating and advancing contact line; the arrows indicate the motion direction of the contact line).

of the heating foil at the same instances are plotted in Fig. 8. At the position of the contact line the heater is cooled down locally. The temperature drop of around 1.5 K is in excellent agreement to the experiment. During its outward motion, the contact line moves towards rather hot parts of the heater. Once the contact line has passed a certain position on the heater, this position is in contact to vapor (no heat transfer) and the temperature starts to rise locally. However, there is not enough time to reach to original level of superheat before the contact line moves back inwards and leads to a local cooling once again. Therefore, the local temperature at the contact line is lower during detachment than during growth. Another interesting aspect is the width of the local temperature minimum. While it is very narrow during growth and at the point of maximum bubble foot diameter, it becomes wider during detachment. This is due to the fact that the liquid–vapor interface moves away from the superheated liquid during detachment (see small pictures in Fig. 8). This leads to an accumulation of colder liquid at the wall and enhances heat transfer by conduction into the liquid next to the contact line. Transient conduction has also been observed experimentally by Demiray and Kim (2004) and Myers et al. (2005) who measured significantly higher heat flux peaks in the case of an advancing contact line (rewetting during detachment). This experimental finding is in excellent agreement to the heat flux data plotted in Fig. 7.

3.3. *Possible sources of error*

Due to the tremendously high complexity of nucleate boiling, the level of agreement that is achieved is very satisfying and confirms the physical correctness of the model. The possible reasons for the remaining differences are numerous. Apart from discretization errors and the lack of precise knowledge of some experimental boundary conditions, the modeling of the contact angle is a possible source of error. In this study, a constant angle has been chosen in the first fluid cell at the wall corresponding to the static contact angle of the fluid-wall system. However, the value is most probably not constant due to the highly dynamic bubble growth and detachment. Even a hysteresis might be possible between advancing and receding situations. The modest deviation of the bubble departure diameter and growth time could be due to this simplification.

The different development of the heat flux peak during detachment of a bubble is most probably due to the measurement technique applied by Wagner et al. (2007). The infrared images are averaged during the exposure time of 1 ms. Together with the signal damping in the heating foil this could lead to a non-detection of the heat flux peak during detachment. On the same setup, the authors used 20 μm foils and detected a significant heat flux peak during detachment (Wagner and Stephan, 2009). The simulation results are not averaged within the exposure time, but provide instantaneous temperature fields. This could possibly explain why the peak is captured by the simulation but not by the experiment. Other experimental studies with a different measurement technique for the wall heat flux (Demiray and Kim, 2004; Myers et al., 2005) support the numerical result of higher heat flux peaks during detachment. Schweizer and Stephan (2009)

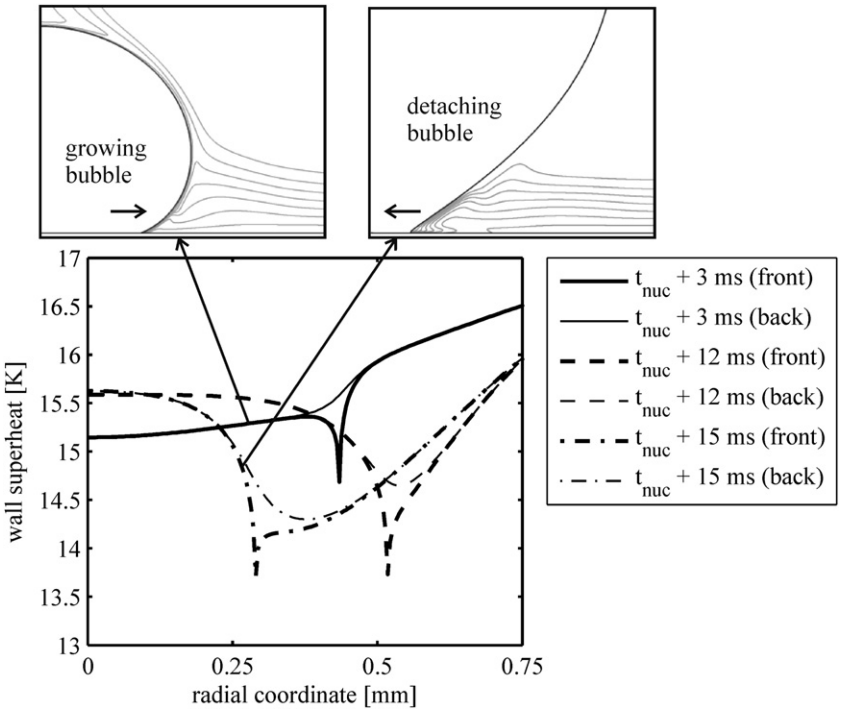

Fig. 8 – Local wall superheat in different situations during bubble growth (receding, stagnating and advancing contact line) on front (solid–fluid interface) and back side (adiabatic) of heating foil.

observed a higher heat flux peak during detachment in an experiment similar to Wagner et al. (2007) in reduced gravity conditions. Possibly, the slower bubble growth in reduced gravity allows for measuring the heat flux peak during detachment while it could be totally or partially masked in earth gravity experiments.

4. Conclusion

The VOF method of the OpenFOAM CFD package has been extended and modified in order to simulate boiling heat transfer. The boiling model incorporates mass, momentum and phase transfer in the fluid, contact line evaporation and the transient heat conduction in the heating wall. It was used to simulate boiling of HFE-7100 at 500 mbar at an artificial nucleation site according to the generic experiments performed by Wagner et al. (2007). The results were compared quantitatively to the experimental observations. Global parameters such as bubble growth time and departure diameter are in reasonable agreement. Thanks to the high spatial and temporal resolution of experiment and simulation, the capability of the boiling model to describe local heat transfer phenomena could be validated. The results on local heat flux and the cooling of the wall at the contact line are in good agreement. The simulations provide deep insight into the boiling process and are therefore a promising approach towards a more comprehensive understanding of the phenomenon.

In future, parts of the model such as contact angle modeling will be extended and the model will also be used for 3-dimensional simulations of flow boiling heat transfer and the effect of bubble mergers on the local heat transfer.

Acknowledgements

The authors would like to thank the German Research Foundation (DFG) for project support.

REFERENCES

Demiray, F., Kim, J., 2004. Microscale heat transfer measurements during pool boiling of FC-72: effect of subcooling. Int. J. Heat Mass Transfer 47, 3257–3268.

Fuchs, T., Kern, J., Stephan, P., 2006. A transient nucleate boiling model including microscale effects and wall heat transfer. J. Heat Transfer 128, 1257–1265.

Hardt, S., Wondra, F., 2008. Evaporation model for interfacial flows based on a continuum-field representation of source terms. J. Comput. Phys. 227, 5871–5895.

Kunkelmann, C., Stephan, P., 2009. CFD simulation of boiling flows using the Volume-of-Fluid method within OpenFOAM. Numer. Heat Transfer A 56, 631–646.

Li, D., Dhir, V.K., 2007. Numerical study of single bubble dynamics during flow boiling. J. Heat Transfer 129, 864–876.

Myers, J.G., Yerramilli, V.K., Hussey, S.W., Yee, G.F., Kim, J., 2005. Time and space resolved wall temperature and heat flux measurements during nucleate boiling with constant heat flux boundary conditions. Int. J. Heat Mass Transfer 48, 2429–2442.

Schweizer, N., Stephan, P., 2009. Experimental study of bubble behaviour and local heat flux in pool boiling under variable gravitational conditions. Multiphase Sci. Technol. 21, 329–350.

Son, G., Dhir, V.K., Ramanujapu, N., 1999. Dynamics and heat transfer associated with a single bubble during nucleate boiling on a horizontal surface. J. Heat Transfer 121, 623–631.

Stephan, P.C., Busse, C.A., 1992. Analysis of the heat transfer coefficient of grooved heat pipe evaporator walls. Int. J. Heat Mass Transfer 35, 383–391.

Sussman, M., Almgren, A.S., Bell, J.B., Colella, P., Howell, L.H., Welcome, M.L., 1999. An adaptive level set approach for incompressible two-phase flows. J. Comput. Phys. 148, 81–124.

Wagner, E., Stephan, P., Koeppen, O., Auracher, H., 2007. High resolution temperature measurements at moving vapor/liquid and vapor/liquid/solid interfaces during bubble growth in nucleate boiling. In: Proc. 4th Int. Berlin Workshop on Transport Phenomena with Moving Boundaries, Berlin, Germany, vol. 260–277. VDI Verlag, ISBN 3-18-388303-1.

Wagner, E., Stephan, P., 2009. High-resolution measurements at nucleate boiling of pure FC-84 and FC-3284 and its binary mixtures. J. Heat Transfer 131, 121008.

Weller, H.G., Tabor, G., Jasak, H., Fureby, C., 1998. A tensorial approach to computational continuum mechanics using object-oriented techniques. Comput. Phys. 12, 620–631.

Wu, J., Dhir, V.K., Qian, J., 2007. Numerical simulation of subcooled nucleate boiling by coupling level-set method with moving-mesh method. Numer. Heat Transfer B 51, 535–563.